


Article

Direct Ink Writing of Highly Conductive and Strongly Adhesive PEDOT:PSS-EP Coatings for Antistatic Applications

Ning Lv ^{1,†}, Shuhan Liu ^{2,†}, Guiqun Liu ^{3,*}  and Ximei Liu ^{2,*}¹ Luzhou Vocational and Technical College, Luzhou 646000, China; shuiwuchang@foxmail.com² Jiangxi Province Key Lab of Flexible Electronics, Flexible Electronics Innovation Institute, Jiangxi Science and Technology Normal University, Nanchang 330038, China; shuhanliu1005@163.com³ School of Materials Science and Technology, North Minzu University, Yinchuan 750021, China

* Correspondence: gqliu10b@alum.imr.ac.cn (G.L.); liuxm@jxstnu.edu.cn (X.L.); Tel.: +86-791-88537967 (X.L.)

† These authors contribute equally to this work.

Abstract: As the information age progresses, the electronics industry is evolving towards smaller and more sophisticated products. However, electrostatic potentials easily penetrate these components, causing damage. This underscores the urgent need for materials with superior antistatic properties to safeguard electronic devices from such damage. Antistatic coatings typically rely on polymers as the primary material, enhanced with conductive fillers and additives to improve performance. Despite significant progress, these coatings still face challenges related to advanced processing technologies and the integration of electrical and mechanical properties. Among various conductive fillers, the conducting polymer PEDOT:PSS stands out for its exceptional conductivity, environmental stability, and long cycle life. Additionally, epoxy resin (EP) is widely utilized in polymer coatings due to its strong adhesion to diverse substrates during curing. Here, we develop highly conductive and strongly adhesive PEDOT:PSS inks by combining PEDOT:PSS with EP using a composite engineering approach. These inks are used to fabricate PEDOT:PSS coatings by direct ink writing (DIW). We systematically evaluate the DIW of PEDOT:PSS-EP coatings, which show high electrical conductivity (ranging from 0.59 ± 0.07 to $41.50 \pm 3.26 \text{ S cm}^{-1}$), strong adhesion (ranging from 15.84 ± 2.18 to $99.3 \pm 9.06 \text{ kPa}$), and robust mechanical strength (8 MPa). Additionally, we examine the surface morphology, wettability, and hardness of the coatings with varying PEDOT:PSS content. The resultant coatings demonstrate significant potential for applications in antistatic protection, electromagnetic shielding, and other flexible electronic technologies.

Keywords: conductive coating; PEDOT:PSS; epoxy resin; direct ink writing; antistatic application

Citation: Lv, N.; Liu, S.; Liu, G.; Liu, X. Direct Ink Writing of Highly Conductive and Strongly Adhesive PEDOT:PSS-EP Coatings for Antistatic Applications. *Colloids Interfaces* **2024**, *8*, 48. <https://doi.org/10.3390/colloids8050048>

Academic Editor: Alexander Kamyshny

Received: 18 July 2024

Revised: 21 August 2024

Accepted: 22 August 2024

Published: 23 August 2024



Copyright: © 2024 by the authors. Licensee MDPI, Basel, Switzerland. This article is an open access article distributed under the terms and conditions of the Creative Commons Attribution (CC BY) license (<https://creativecommons.org/licenses/by/4.0/>).

1. Introduction

With the continuous advancement of the information age, the field of flexible electronics has rapidly developed, showing significant potential for applications in electronic components, smart electronic products, wearable devices, and medical equipment [1–3]. However, as the electronics industry continues to develop towards smaller and more precise components, the antistatic and electromagnetic shielding capabilities of electronic products have diminished. This reduction in protective capabilities allows electrostatic potential to more easily penetrate and damage electronic components. Consequently, the likelihood of electrostatic discharge causing harm to electronic products has increased [4,5]. Single-function flexible electronic devices are increasingly insufficient for complex application scenarios. Therefore, there is an urgent need to develop materials with excellent antistatic properties and electromagnetic shielding capabilities to protect electronic products from electrostatic damage.

Antistatic coatings typically consist of polymers as the base material, along with functional additives such as conductive fillers or antistatic agents to impart antistatic properties [6,7]. Among many conductive fillers, conducting polymers stand out as star

materials due to their excellent electrical properties [8,9], electrochemical and environmental stability [10,11], good redox activity, and long cycle life [12,13]. Although significant progress has been achieved, such as the preparation of aqueous nanostructure-modified conductive coatings by blending polypyrrole with polyurethane and the development of corrosion-resistant and antistatic organic coatings by compositing polypyrrole with epoxy resin, there are still opportunities for further enhancement and exploration in this field [14–17]. However, challenges like insufficient coating adhesion and difficulties in advanced processing techniques still remain.

PEDOT (poly(3,4-ethylenedioxythiophene)) is an excellent conductive polymer known for its small energy gap, low oxidation potential, and high conductivity. However, its inherent ‘insoluble and refractory’ characteristics limit its processability in subsequent applications [18]. Water-soluble PSS (polystyrene sulfonic acid) is the most commonly used dopant for PEDOT. When PEDOT is doped with PSS, the non-water-soluble PEDOT conductive molecular chains combine with the strongly hydrophilic PSS chains to achieve charge balance. This results in stable dispersion in water, allowing PEDOT:PSS ink to be coated on different substrates and dried to form films. This improves the processing performance significantly. The structure of PEDOT:PSS includes a PSS polymerization chain that is inherently insulating. Upon drying, the film particles exhibit a core-shell morphology where PEDOT is enriched in the core and PSS in the shell. This configuration limits the conductivity of PEDOT:PSS inks, often falling short of practical application requirements [19,20]. By incorporating specific conductive additives, the surface structure and performance of PEDOT:PSS films can be precisely tailored. For instance, Lu et al. discovered that dimethyl sulfoxide (DMSO) as a dopant not only markedly enhanced the electrical conductivity of PEDOT:PSS inks but also improved the morphology, interfacial contact, and other key properties of PEDOT:PSS films [21,22]. Although there have been related reports, they primarily focused on the design and application of new PEDOT:PSS composite inks [23–25]. In addition to conductivity, the stability of PEDOT:PSS ink is crucial for its film-forming properties. To enhance both the mechanical properties and stability of PEDOT:PSS films, resin is often added as a film-forming substance in the ink formulation. The introduction of epoxy resin (EP) into the system can promote the aggregation and deposition of charged colloids, thereby improving conductivity, adhesion, and processability. At the same time, EP molecules contain reactive epoxy, hydroxyl groups, and other polar groups. These can react with hydroxyl, amine, and other reactive functional groups on the substrate surface, forming chemical bonds that significantly enhance adhesion [26,27]. Based on the aforementioned performance advantages, PEDOT:PSS-based conductive materials have been developed and applied in various fields, such as flexible sensors [28,29], soft robots [30,31], flexible electronics [32,33], wound healing [34,35], and bioelectronics [36,37]. We speculate that these materials may also hold promising application prospects in fields related to antistatic coatings and electromagnetic shielding.

Here, highly conductive and strongly adhesive PEDOT:PSS-EP inks are prepared by blending PEDOT:PSS with adhesive EP using a composite engineering strategy. We fabricated PEDOT:PSS-EP coatings using DIW and systematically studied various properties, including printability, electrical conductivity, adhesion, mechanical strength, surface morphology, surface wettability, and surface hardness. We explored how these properties vary with different PEDOT:PSS content in the coatings. The prepared PEDOT:PSS-EP coatings hold significant promise for advancing the application of PEDOT:PSS materials in various fields, such as antistatic protection, electromagnetic shielding, and flexible electronic products. These developments may also have substantial potential for further commercialization and widespread use.

2. Materials and Methods

2.1. Materials

Poly(3,4-ethylenedioxythiophene):polystyrene sulfonate (PEDOT:PSS, Kaivo, Zhuhai, China), dimethyl sulfoxide (DMSO, >99.8%, Aladdin, Shanghai, China), bisphenol A epoxy

resin emulsion (epoxy equivalent weight of 1010), and a curing agent (configured in the following volume ratio (propylene glycol methyl ether:water:ethylenediamine = 5:2:13, $v/v/v$) were used. All reagents and chemicals were not further purified.

2.2. Preparation of PEDOT:PSS-EP Precursor Ink

PEDOT:PSS, DMSO, bisphenol A epoxy resin emulsion, and a curing agent were used as received without further purification [38]. Firstly, 0.5 g of pure PEDOT:PSS conductive fibers were dispersed in 9.5 g of DMSO mixture (DMSO:water = 15:85, w/w). The PEDOT:PSS aqueous dispersion of 5 wt% (w/w) was obtained by thorough mixing with a syringe. To prepare various concentrations of PEDOT:PSS-EP inks, the 5 wt% PEDOT:PSS aqueous dispersion was mixed with the EP emulsion in the mass ratios of 4:6, 5:5, 6:4, 7:3, 8:2, and 9:1 (PEDOT:PSS/EP), corresponding to PEDOT:PSS contents of 40%, 50%, 60%, 70%, 80%, and 90%, respectively. After ensuring uniform mixing with the syringe, an ethylenediamine curing agent was added to the PEDOT:PSS-EP mixture at a ratio of 0.1:2.6 (curing agent:EP, w/w). The mixture was thoroughly mixed again to obtain the ink.

2.3. DIW of PEDOT:PSS-EP Precursor Ink

DIW of PEDOT:PSS-EP precursor ink was accomplished using a DB 100 3D printing system from Shanghai Mifang Electronic Technology, Shanghai, China, equipped with stainless steel nozzles ranging from 90 to 340 μm in diameter. This printer operated under atmospheric pressure conditions and was capable of achieving print shapes under pressures ranging from 0 to 500 kPa. The models required for printing were initially designed using Adobe Illustrator 2020 (Adobe, San Jose, CA, USA), to ensure they met printing specifications, and they were saved in SVG format. These SVG files were then imported into the control software of the 3D printer, where additional adjustments to the models could be made as needed before printing. The base was positioned on the print bed, and the printing material was loaded into the material chamber of the 3D printer, ensuring proper loading and nozzle clearance. Once the printing parameters were adjusted, the printing process commenced smoothly. The thickness of the printed PEDOT:PSS-EP coating was approximately 0.5 mm before drying. After drying at 60 °C for 24 h, the thickness of the coating was about 100 μm . Under the drying conditions of 60 °C for 24 h, the PEDOT:PSS-EP coating not only ensured that the solvents were fully evaporated, but also facilitated the crosslinking and curing of the epoxy resin.

2.4. Electrical Conductivity Test

The electrical conductivity of the PEDOT:PSS-EP coating was measured using the four-point probe method. A constant electric current was applied between the outer two probes using an external power source. This method ensures accurate measurement by minimizing errors from contact resistance, providing reliable data on the coating's conductivity. The conductivity test samples were rectangular PEDOT:PSS-EP coatings prepared by DIW, with each sample's length, width, and thickness individually measured. The resistance (R) between the inner two probes was measured using a Keithley 2700 digital multimeter (Keithley, Cleveland, OH, USA). Based on the measured resistance value and the geometric parameters between the probes, the resistivity of the sample was calculated. The geometric parameters between the probes include: the thickness of the sample (T), which was measured using a micrometer, and the length (L) and width (W), which were measured using a vernier caliper; their electrical conductivity (σ) was calculated using the following formula:

$$\sigma = \frac{L}{WRT} \quad (1)$$

2.5. Adhesion Performance Test

To evaluate the adhesive strength, we conducted a standardized lap shear strength test using a ZQ-990LB mechanical testing machine from ZHIQU Precision Instruments

(Dongguan ZHIQU Precision Instrument Co., Ltd., Dongguan, China). For preparing the PEDOT:PSS-EP coating lap shear samples, two identical substrates of the same material and size were used. The sample was applied to one of the substrates, ensuring a uniform and consistent coating thickness across the entire lap joint area. The other substrate was then carefully attached, making sure that both surfaces were in full contact, with no bubbles or gaps, to ensure a secure bond. A specific pressure was applied to the assembled samples to ensure even distribution and optimal bonding. The samples were placed in an oven set at 65 degrees Celsius for 12 h for heat curing. The length and width of the prepared samples were measured using a vernier caliper to calculate the bonding area accurately. Then, the samples were placed on the mechanical testing machine and subjected to testing at a constant pulling speed of 50 mm/min. The lap shear strength was calculated by dividing the maximum force by the bonding area, using the following formula [39–41]:

$$\text{Lap shear strength} = \frac{F_{max}}{S} \quad (2)$$

where F_{max} and S represent the maximum force and the adhesion area during the lap shear test, respectively [42].

The adhesion grade of the PEDOT:PSS-EP coating was tested using a cross-cut tester (503, BIUGED Precision Instrument Co., Ltd., Guangzhou, China). The PEDOT:PSS-EP coating and its substrate (PI) were prepared for testing. After drying the surface of the PEDOT:PSS-EP coating, it was ensured to be clean and free of any impurities. The cross-cut tester was placed on the coating, aligning the gaps horizontally and vertically. A surgical blade was used to make a cross-shaped incision along the gaps in the cross-cut tester. Adhesive tape was applied over the cross-shaped incision and quickly peeled off. The integrity of the coating was observed (Grade 0: the cut edges were completely smooth, with no squares detached; Grade 1: slight detachment of the coating at the intersection of the incision, with the affected area not significantly greater than 5% of the intersection area; Grade 2: detachment of the coating at the intersection and/or along the edges of the incision, with the affected intersection area significantly greater than 5% but not more than 15%; Grade 3: partial or complete detachment of the coating along the edges of the incision or in different parts of the squares, with the affected intersection area significantly greater than 15% but not more than 35%; Grade 4: large pieces of coating detached along the edges of the incision or partial or complete detachment of some squares, with the affected intersection area significantly greater than 35% but not more than 65%; Grade 5: detachment exceeding 65%). Multiple measurements were performed and the results of each measurement were recorded.

2.6. Morphological Characterization

The morphology of the PEDOT:PSS-EP coatings were observed using a metallographic microscope (LW300LJT, Beijing Cewei Optoelectronic Technology Co., Ltd., Beijing, China). Before observation, the microscope was cleaned, and the lenses were checked to ensure they were spotless. The light source was turned on and the brightness was adjusted to suitable levels for optimal observation. The PEDOT:PSS-EP coating was placed on the microscope stage and secured with a fixation device. The coarse focus wheel was used to bring the coating into focus, and the focal length was gradually adjusted with the fine focus wheel until the PEDOT:PSS-EP coating was clearly visible. The coating was observed through the microscope eyepiece, with the focal length and magnification adjusted as needed until the desired details were clearly visible. The microscope's position was adjusted to change the field of view as required. The morphology of the observed PEDOT:PSS-EP coating was documented, and images were captured as necessary.

2.7. Water Contact Angle

The contact angle of the PEDOT:PSS-EP coating was measured using a water contact angle (WCA) goniometer (SDC-100, Dongguan Shengding Precision Instrument Co., Ltd.,

Dongguan, China). To ensure accurate measurement, the surface of the PEDOT:PSS-EP coating was thoroughly cleaned before testing. The PEDOT:PSS-EP coating to be tested was placed on the horizontal platform of the contact angle goniometer. The surface of the PEDOT:PSS-EP coating was ensured to be free of dust and other impurities. Using a micropipette (1 mL), a droplet of liquid was carefully dispensed onto the surface of the PEDOT:PSS-EP coating, ensuring the droplet size was uniform and stable and avoiding any spreading or splashing. Images of the droplet interface with the PEDOT:PSS-EP coating surface were captured using a contact angle goniometer. The contact angle between the droplet and the PEDOT:PSS-EP coating surface in the captured images was analyzed using the goniometer's configured software. Multiple measurements were conducted, and the results of each measurement were recorded [43].

2.8. Pencil Hardness

The hardness of the PEDOT:PSS-EP coating was measured using pencils (Pencil 9800, Mitsubishi, 6B-9H, Tokyo, Japan) and a carriage-type pencil hardness tester (BGD506/2, BIUGED Precision Instrument Co., Ltd., Guangzhou China). To perform this test, the PEDOT:PSS-EP coating was prepared, and a series of pencils was arranged for the measurement. The surface of the PEDOT:PSS-EP coating was ensured to be clean, free of impurities, and undamaged. The coating was placed on a level tabletop. Selected pencils of different hardness levels were mounted on a carriage-type pencil hardness tester, where they were allowed to traverse the PEDOT:PSS-EP coating and leave a trace. To determine the pencil that best matched the hardness of the PEDOT:PSS-EP coating, the depth and texture of the pencil marks on the coating were observed. The hardness level that corresponded most closely to the coating scratch was recorded each time, using standard pencil hardness ratings (such as 4H, B, 6B, etc.). Multiple measurements were conducted, and the results for each instance were documented.

2.9. Glossiness Testing

The glossiness of the PEDOT:PSS-EP coating was measured using a gloss meter (BGD 516/3, BIUGED Precision Instrument Co. Ltd.). The PEDOT:PSS-EP coating to be tested was prepared, ensuring its surface was clean, dust-free, and free of impurities. The gloss meter was turned on, ensuring it was in working condition and properly calibrated. The parameters for glossiness testing were set, using a testing angle of 60 degrees. The PEDOT:PSS-EP coating was placed on the gloss meter, ensuring its surface was perpendicular to both the light source and the detector. The gloss meter was started to begin the testing process. During the measurement, care was taken to ensure that the surface of the PEDOT:PSS-EP coating was not disturbed by external factors such as vibration. Multiple measurements were performed, and the results of each measurement were recorded.

3. Results

3.1. Design of DIW Printable PEDOT:PSS-EP Inks

Ideal antistatic coatings should possess the following characteristics: (1) Electrical conductivity: antistatic coatings should exhibit excellent electrical conductivity to efficiently dissipate or conduct static charges to the ground, minimizing static buildup. (2) Mechanical strength: the coatings are designed for surface protection, requiring robust mechanical strength and abrasion resistance to withstand friction, abrasion, and scratches. (3) Excellent adhesion: ensuring excellent adhesion is crucial for these coatings, allowing them to firmly adhere to the substrate surface without flaking or peeling off easily. (4) Processability: these coatings exhibit excellent processability, allowing them to be easily applied to substrates of various shapes and surfaces. This versatility ensures them to meet diverse application requirements effectively [44–46].

To design high-performance antistatic coatings, we prepared inks by blending conducting polymer PEDOT:PSS nanofibers with an adhesive macromolecule EP using a composite engineering approach. We added curing agents to these inks to create reactive curing

hybrid inks (Figure 1b). Subsequently, the hybrid ink was applied to various substrates using DIW technology (Figure 1a). When heat is applied, the curing agent in the ink reacts with the epoxy groups within the EP molecules, forming a crosslinked structure that cures the liquid epoxy ink into a hardened coating. In this high-performance antistatic coating, the highly conductive PEDOT:PSS nanofibers ensure excellent electrical properties. Meanwhile, the EP, which contains highly reactive epoxy groups, contributes robust mechanical properties and strong adhesion to the coating. The adhesion principle of EP involves both physical adsorption and chemical bonding with the substrate surface. Epoxy groups in EP can physically adsorb to the substrate surface through interaction forces like Van der Waals forces, providing initial adherence strength. Additionally, these epoxy groups can chemically react with reactive groups on the substrate surface (e.g., hydroxyl, amine groups) to form covalent bonds. This chemical bonding is the primary mechanism for achieving high adhesion strength and durability (Figure 1c).

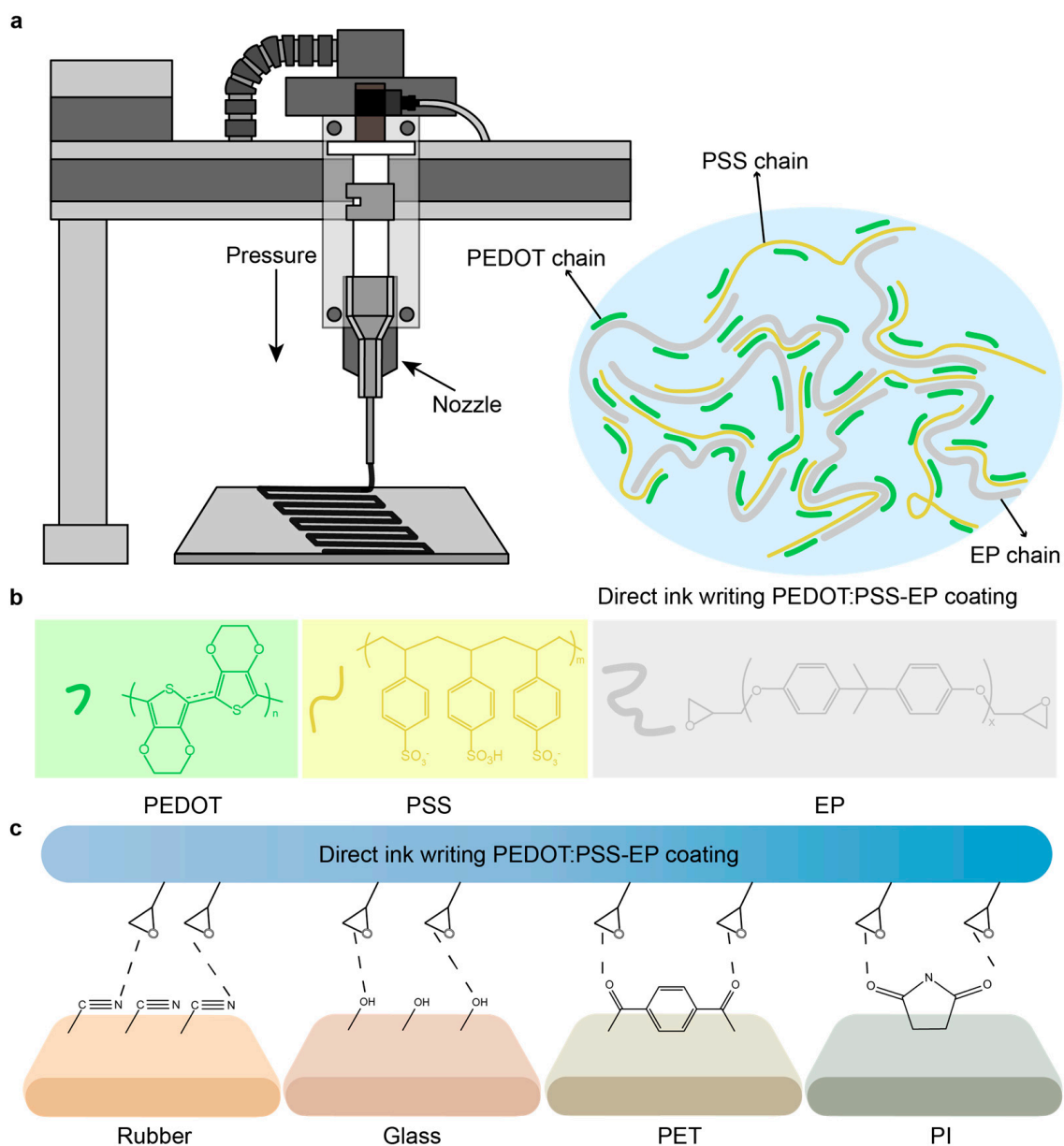


Figure 1. Design of PEDOT:PSS-EP coating by DIW. (a) DIW and thermal curing mechanism of PEDOT:PSS-EP coating. (b) Composition of PEDOT:PSS-EP coating, including PEDOT:PSS and EP. (c) Possible bonding mechanisms of PEDOT:PSS-EP coatings against different substrates.

3.2. DIW of PEDOT:PSS-EP Coating

To demonstrate the smooth DIW of the prepared PEDOT:PSS-EP inks, different ratios of inks (40–90% PEDOT:PSS) were prepared by varying the percentage of PEDOT:PSS solid content in the whole ink, and the effects of parameters such as ink concentration (40–90%), printing pressure (50–500 kPa), and printing tip size (90–340 μm) on the printing performance were investigated. As depicted in Figure 2a, precursor inks with varying PEDOT:PSS solid contents are readily prepared by blending the conducting polymer PEDOT:PSS with EP and curing agent. This process involves mechanical mixing, homogenization, and centrifugation to eliminate air bubbles. The viscosity and energy storage modulus of the resulting inks increase with increasing PEDOT:PSS content. This is due to the higher ink concentration, which increases the internal friction and hence the viscosity. Moreover, their flowability and fidelity to the ink shape are also heightened with increasing ink concentration, demonstrating distinct smoothable DIW properties.

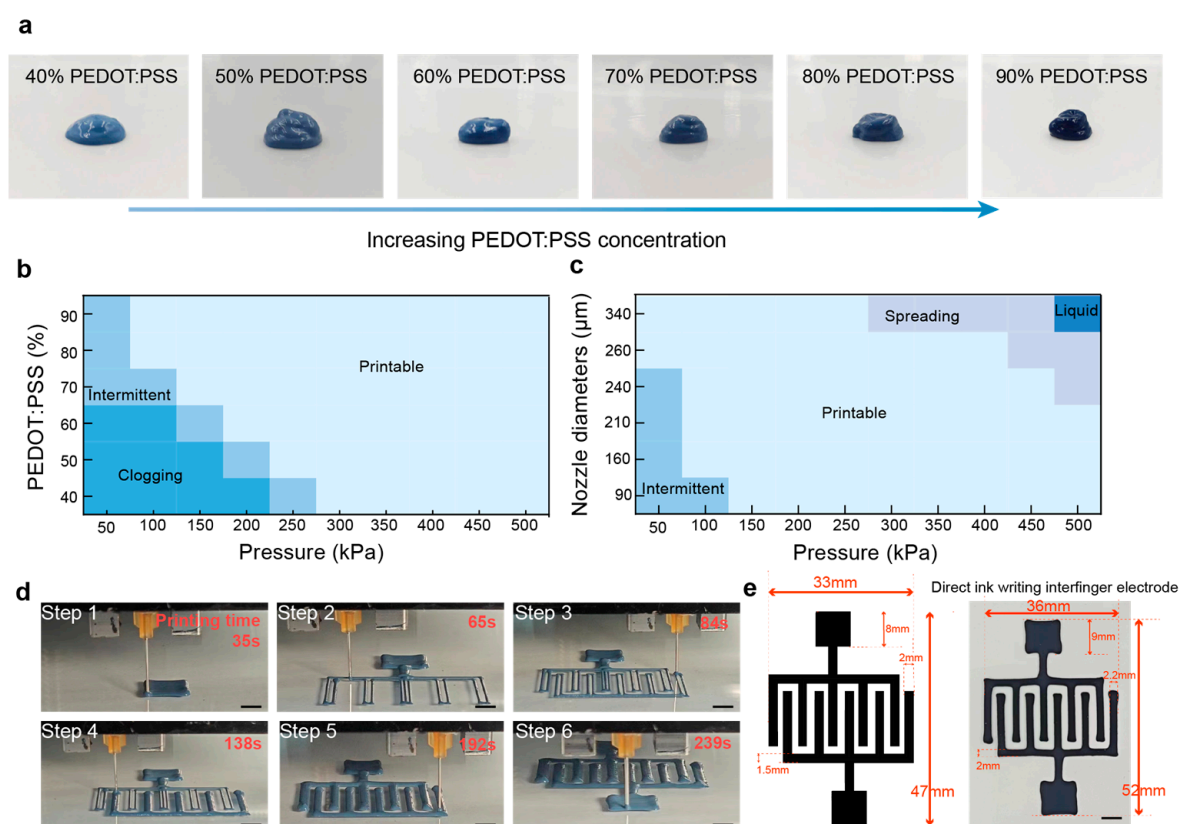


Figure 2. DIW of PEDOT:PSS-EP coating. (a) DIW inks with different concentrations of PEDOT:PSS. (b) The influence of different pressures and different percentages of PEDOT:PSS on the printability of DIW. (c) The influence of different pressures and different nozzle diameters on the printability of DIW. (d) Step-by-step images of printing fork-shaped electrodes on PET substrate. (e) Design diagram and actual image of the interdigitated electrode. Scale bars: 5 mm (d,e).

Note that at a higher EP content (40% PEDOT:PSS), the ink concentration appears lower, and its flow is better. However, its DIW printability is poor, exhibiting problems such as ink clogging the needle and print discontinuities in areas with lower pressures (<150 kPa) and smaller printing needles (<240 μm). This is due to the high cohesion of the highly concentrated EP and its high viscosity, making it difficult to extrude the ink uniformly at low air pressures and with fine needles. In addition, when the EP content is very low, higher print air pressures and thicker print needles can cause lateral spreading of the ink onto the substrate, leading to poorer shape fidelity, primarily due to weak cohesion. Optimal results are achieved with PEDOT:PSS solids in the range of 50–80%, print air pressures between

200 and 400 kPa, and print head sizes ranging from 160 to 260 μm . These conditions produce antistatic coatings with better shape fidelity and a homogeneous, continuous pattern (Figure 2b,c). This can be attributed to the synergistic effect of multiple molecular interactions, including chain entanglement, inter/intramolecular hydrogen bonding, and electrostatic interactions present in the PEDOT:PSS-EP ink. In order to further explore the printing parameters of PEDOT:PSS-EP coating, the printing parameters were optimized by quantifying the printing line width of the same ink with the printing speed, nozzle size, and printing pressure as variables. A quantitative comparison of the printed linewidths was performed at different print speeds (1, 3, 5, 7, and 9 mm s^{-1}), print pressures (100, 200, 300, 400, and 500 kPa), and nozzle diameters (90, 160, 210, and 240 μm) (Figure S1). Similar to the experiments where print speed is the variable, ink width is also positively correlated with needle size and print air pressure. In contrast, the smaller the needle, the lower the pressure, and the faster the print rate, the narrower the line width and the higher the print accuracy. The highest accuracy of printing is up to about 100 μm (Figure S1a), with the possibility of realizing high-precision printing. With the optimized printing parameters and using inks prepared with 70% solid content at 300 kPa and 240 μm size, we successfully printed finger-inserted electrodes (Figure 2d). A finger electrode was designed with an initial length of 47 mm and a width of 33 mm. The inserted finger section was specified to be 2 mm wide, with the two ends featuring a square structure with a width of 8 mm. After machining and molding, the actual dimensions were measured as follows: the length was 52 mm, the width was 36 mm, the inserted finger section was 2.2 mm wide, and the ends were 9 mm wide. The precise dimensions are shown in Figure 2e. The water content of PEDOT:PSS-EP coatings decreases with increasing solids content and remains stable after full cross-linking and curing (Figure S2). Even when immersed in water for up to ten days, there is no shape expansion or contraction (Figure 2e). At the same time, the printed PEDOT:PSS-EP coating has a thickness of about a 100 μm when fully cured and dried (Figure S3), which is close to the thickness of commercially available antistatic coatings (Table S2). These results highlight the applicability and stability of the prepared ink for antistatic coatings, paving the way for practical applications in electronic devices and potential marketability.

3.3. Conductivity and Mechanical Properties of PEDOT:PSS-EP Coating

It is demonstrated that a series of inks with tunable rheological properties can be easily obtained by varying the ratio of PEDOT:PSS to EP (Figure 2a). All inks with different PEDOT:PSS content show significant shear-thinning properties, which allows the inks to be extruded smoothly during the DIW process (Figure 3a). The introduction of EP into PEDOT:PSS generally increases the viscosity of PEDOT:PSS-EP inks. The electrical, mechanical, and adhesion properties of PEDOT:PSS-EP coatings were systematically investigated across various PEDOT:PSS concentrations (40–90%) to optimize antistatic coatings for enhanced performance. As anticipated, the electrical conductivity of the PEDOT:PSS-EP coatings increases with higher PEDOT:PSS content, ranging from $0.59 \pm 0.07 \text{ S cm}^{-1}$ at 40% PEDOT:PSS to $41.50 \pm 3.26 \text{ S cm}^{-1}$ at 90% PEDOT:PSS (Figure 3c). It is noteworthy that the exponential increase in conductivity beyond 70% PEDOT:PSS content is not solely due to the increased PEDOT:PSS content alone. The presence of a small amount of EP likely contributes through a doping effect. During thermal curing, EP facilitates chain rearrangement within PEDOT:PSS. This process tightly binds non-conductive PSS chains to EP, forming a solid and robust structure. The non-conducting PSS chains tightly bind to the EP, forming a robust coating network. Meanwhile, the conductive PEDOT creates a PEDOT-enriched region, enhancing electron circulation and exponentially increasing conductivity. As the PEDOT:PSS content rises, adhesion between the coating and the PI substrate decreases, yet with just 10% EP, adhesion still reaches Grade 2, demonstrating excellent bonding (Figure 3d). In addition, the mechanical properties of the coatings play a crucial role in assessing long-term stability and resistance to tensile and scratch forces. We conducted standard tensile tests to measure the stress during the tensile process, revealing that both

stress magnitude and Young's modulus of the coatings increase with higher PEDOT:PSS content (Figure 3e,f). This trend may be attributed to the inhomogeneous dispersion of high EP content in the composite system, leading to aggregation or agglomeration phenomena. Such uneven distribution can result in localized stress concentrations, thereby reducing the overall toughness and mechanical properties of the coating. Furthermore, we examined the adhesion strength between the PEDOT:PSS-EP coating and various substrates using lap shear tests (Figure 3g), yielding the following values: glass (15.84 ± 2.18 kPa), rubber (16.92 ± 2.71 kPa), PE (24.88 ± 5.33 kPa), Al (33.4 ± 2.18 kPa), PET (71.47 ± 6.56 kPa), and PI (99.3 ± 9.06 kPa) (Figure 3h). Compared to the state-of-the-art progress, our PEDOT:PSS-EP coating exhibits superior performance in both the conductivity and adhesion strength (Figure 3i). These excellent adhesion properties and conductivity are expected to further facilitate the commercialization of PEDOT:PSS-EP coatings.

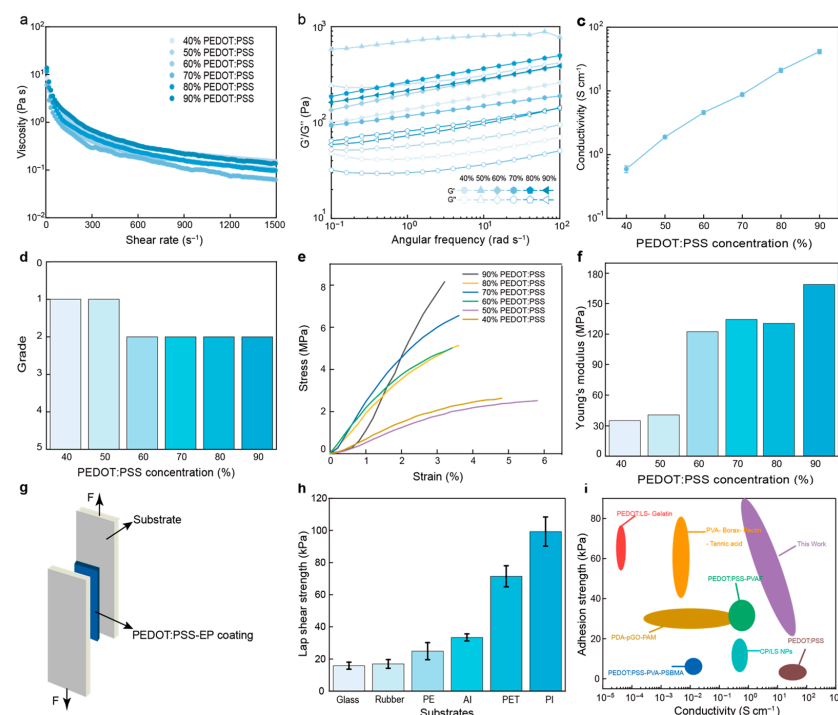


Figure 3. Rheological, conductivity, and mechanical properties of PEDOT:PSS-EP coatings. (a) Apparent viscosity of PEDOT:PSS-EP-based ink as a function of shear rate. (b) Shear storage modulus as a function of shear angle frequency. (c) The influence of different concentrations of PEDOT:PSS on conductivity ($n = 3$). (d) The effect of different concentrations of PEDOT:PSS on the adhesion to PI substrate. (e) Stress-strain curves under different concentrations of PEDOT:PSS. (f) Young's modulus at different concentrations of PEDOT:PSS. (g) Lap shear model. (h) Adhesive strength measured through lap shear experiments at different concentrations of PEDOT:PSS ($n = 3$). (i) Comparison of adhesion strength and conductivity with previously reported works on PEDOT:PSS-based coatings.

3.4. Topography of PEDOT:PSS-EP Coating

Surface morphology plays a crucial role in the long-term stability and performance of coatings. A smooth and uniform surface enhances aesthetics by reflecting light evenly, giving the coating a flat and consistent appearance. Moreover, surface topography directly influences functional performance; for instance, in protective coatings, a smooth surface provides better defense against environmental erosion and substrate damage. Surface topography plays a crucial role in assessing the functionality of coatings. By analyzing the surface topography, we can evaluate the quality, performance, and stability of the coating. This analysis provides a valuable reference for optimizing coating design.

To analyze the surface topography of the PEDOT:PSS-EP coating, we captured micrographs using a microscope in two modes: bottom light source and top light source. Figure 4a illustrates that all scales of the PEDOT:PSS-EP coatings, when observed under the bottom light source, exhibit uniform, similar, and compact morphology. This suggests homogeneous mixing of PEDOT:PSS with EP in the coating (Figure 4a). Similarly, when we switched the illumination source of the microscope from the bottom to the top, we observed that composite coatings with higher EP content exhibit a rougher surface and poorer surface conductivity. This roughness may be attributed to the agglomeration of EP at high concentrations. Interestingly, PEDOT:PSS-EP coatings show a denser and more uniform morphology as the PEDOT:PSS content increases (Figure 4b). This phenomenon could arise from the tendency of low-concentration PEDOT:PSS macromolecular chains to aggregate into large spherical composite particles during drying, leading to improved leveling of the coating. This process relies on the reaction between the EP and the amine curing agent, along with ensuring good compatibility between the cured EP and PEDOT:PSS. However, the deep entanglement of non-conductive EP chains and the encapsulation of PEDOT:PSS molecular chains can hinder the formation of conductive pathways.

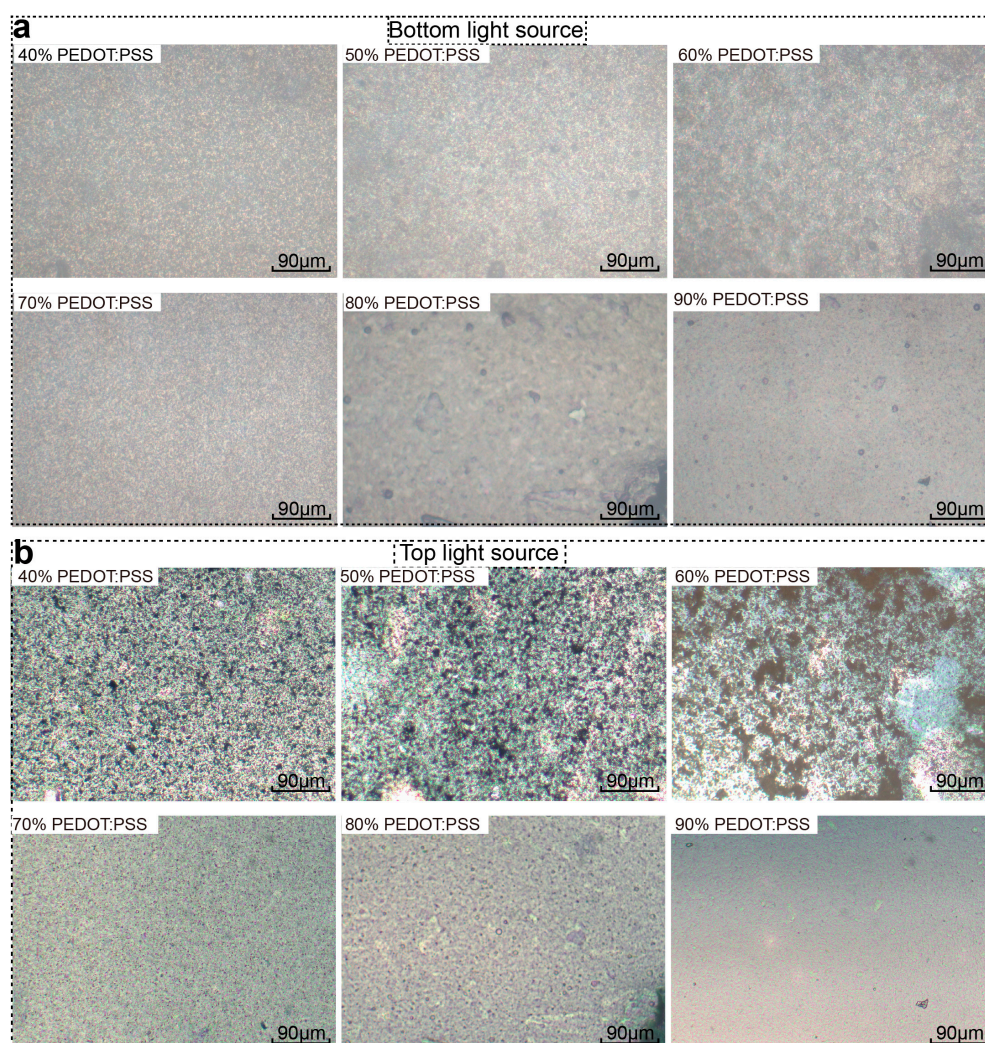


Figure 4. Microscope morphology photos of PEDOT:PSS-EP coating. (a) Microscope morphology photos of PEDOT:PSS-EP coatings (bottom light source) with different PEDOT:PSS concentrations. (b) Microscope morphology photos of PEDOT:PSS-EP coatings (top light source) with different PEDOT:PSS concentrations. Scale bars: 90 μm (a,b).

3.5. DIW of PEDOT:PSS-EP Coating for Abrasion Performance and Surface Properties

Surface wettability, hardness, and gloss are crucial parameters influencing the performance of coatings. In our study, we investigated how the structure of coatings formed by curing different ratios of EP with PEDOT:PSS affects these properties. The surface wettability of PEDOT:PSS-EP coatings is theoretically influenced by both surface roughness and surface energy. A rougher surface and a lower surface energy at the interface typically result in a more hydrophobic interface. These factors are integral to optimizing the performance of PEDOT:PSS-EP coatings in various applications. As the PEDOT:PSS content increased from 40% to 90%, we observed a gradual decrease in the contact angle size (Figure 5a,b), which correlates with the interface roughness observed in micrographs. Higher PEDOT:PSS content led to coatings with smaller roughness and a more uniform surface, exhibiting increased hydrophilic properties. This can be attributed to the higher presence of strongly hydrophilic PSS chains within the coating interface. Furthermore, consistent with previous studies, higher EP content resulted in greater coating hardness, as depicted in Figure 5c. This increase in EP content caused the pencil hardness to decrease from a B rating to a 4B rating (Figure 5c). Finally, we also explored the glossiness of the coated surface. The ratio of reflected light under incident light at a 60-degree angle for the PEDOT:PSS-EP coatings gradually increases with the PEDOT:PSS content (Figure 5d). This increase in glossiness can be attributed to the flat and smooth surface of the coatings, as well as reduced scattering between the coatings and the substrate, allowing light to reflect more uniformly. The PEDOT:PSS-EP coatings exhibit high electrical conductivity, strong adhesion, and excellent interfacial properties, which are expected to facilitate the use of PEDOT:PSS-EP inks in applications such as antistatic and electromagnetic shielding.

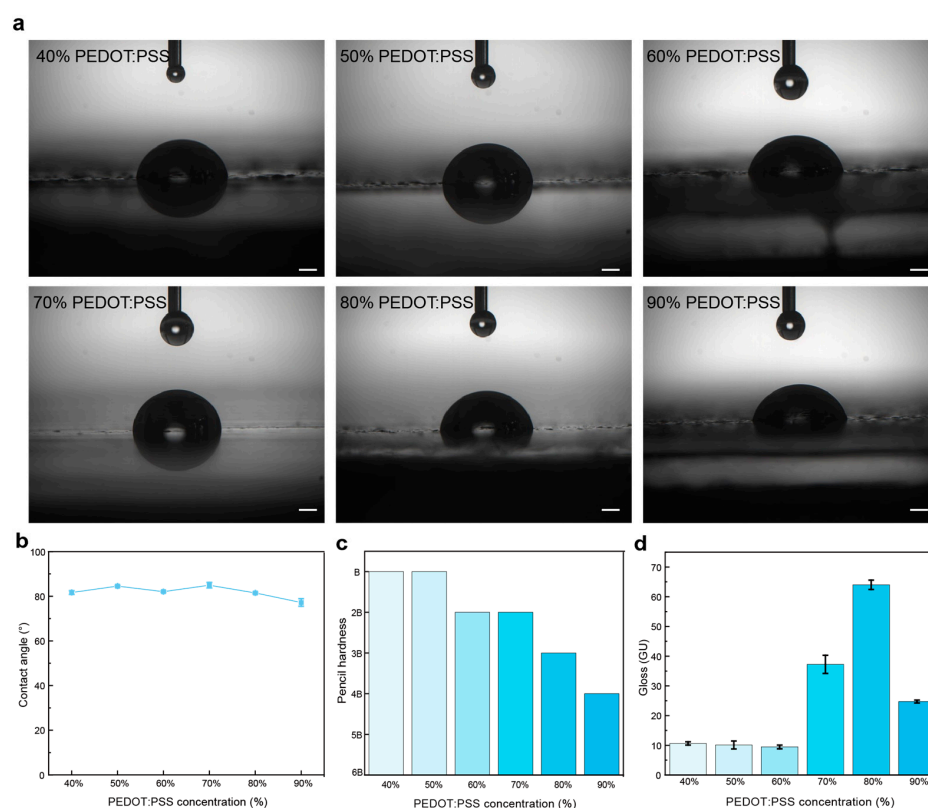


Figure 5. PEDOT:PSS-EP coating for abrasion performance and surface properties. (a) Microscope morphology photos of WCAs of PEDOT:PSS-EP coating with different PEDOT:PSS concentrations. (b) WCAs of PEDOT:PSS-EP coating with different PEDOT:PSS concentrations (n = 3). (c) Pencil hardness of PEDOT:PSS-EP coating with different PEDOT:PSS concentrations. (d) Gloss of PEDOT:PSS-EP coating with different PSS concentrations (n = 3). Scale bars: 450 μ m (a).

4. Conclusions

In this study, we successfully developed high-performance precursor ink based on the conductive filler PEDOT:PSS and macromolecular EP. This composite ink enables the precise fabrication of high-resolution patterns using direct ink DIW technology across a range of printing parameters. The resulting PEDOT:PSS-EP coating exhibits high conductivity, strong adhesion, high fracture toughness, and hardness, making it resistant to pulling, stretching, scratches, and other stresses during use. Additionally, the printed coating exhibits smoother surface topography and higher gloss properties, which collectively enhance the potential advantages of PEDOT:PSS-EP coatings for antistatic and electromagnetic shielding coatings. This work not only advances the development of high-performance, conductive polymer inks but also introduces a promising coating material for providing antistatic protection and electromagnetic shielding in electronic products.

Supplementary Materials: The following Supporting Information can be downloaded at: <https://www.mdpi.com/article/10.3390/colloids8050048/s1>, Figure S1. The relationship between diameter and printing speed for the same ink printed using 90 (a), 160 (b), 210 (c), and 240 μm (d) needles at different pressures (100, 200, 300, 400, and 500 kPa). (n = 3). Figure S2. Water content data for mixtures with different ratios. (n = 3). Figure S3. Comparison of coating thickness before and after drying in a 60 °C oven for 24 h. Table S1. Comparison of conductivity and adhesion strength of published PEDOT:PSS-based coatings. Table S2. Comparison of commercial antistatic film thickness with that of this work.

Author Contributions: Conceptualization, N.L. and X.L.; experiment, N.L. and S.L.; investigation, S.L. and X.L.; writing-original draft, N.L.; writing-review and editing, N.L. and S.L.; data curation, N.L., S.L. and X.L.; funding acquisition, N.L., G.L. and X.L.; supervision, X.L. All authors have read and agreed to the published version of the manuscript.

Funding: This work was financially supported by the Natural Science Foundation of Jiangxi Province (20232BAB202044) provided by Ximei Liu.

Data Availability Statement: The original contributions presented in the study are included in the article/supplementary material, further inquiries can be directed to the corresponding authors.

Conflicts of Interest: The authors declare no conflicts of interest.

References

1. Sangermano, M.; Pegel, S.; Potschke, P.; Voit, B. Antistatic epoxy coatings with carbon nanotubes obtained by cationic photopolymerization. *Macromol. Rapid Commun.* **2008**, *29*, 396–400. [[CrossRef](#)]
2. Li, H.; Lee, H.; Kang, J.; Lim, S. Three-dimensional polymer-nanoparticle-liquid ternary composite for ultrahigh augmentation of piezoelectric nanogenerators. *Nano Energy* **2023**, *113*, 108576. [[CrossRef](#)]
3. Chang, C.; Hwang, F.; Hsieh, C.; Chen, C.; Cheng, L. Preparation and characterization of polymer/zirconia nanocomposite antistatic coatings on plastic substrates. *J. Coat. Technol. Res.* **2013**, *10*, 73–78. [[CrossRef](#)]
4. Zhao, T.; Zhang, C.; Du, Z.; Li, H.; Zou, W. Functionalization of AgNWs with amino groups and its application in epoxy matrix in antistatic and thermal conductivity nanocomposites. *RSC Adv.* **2015**, *5*, 91516–91523. [[CrossRef](#)]
5. Barrau, S.; Demont, P.; Maraval, C.; Bernes, A.; Lacabanne, C. Glass transition temperature depression at the percolation threshold in carbon nanotube-epoxy resin and polypyrrole-epoxy resin composites. *Macromol. Rapid Commun.* **2005**, *26*, 390–394. [[CrossRef](#)]
6. Pradhan, S.; Shubhadarshinee, L.; Mohapatra, P.; Mohanty, P.; Jali, B.; Mohapatra, P.; Barick, A. Conducting polymer composites for antistatic application in aerospace. *Def. Technol.* **2020**, *16*, 107–118.
7. Song, N.; Pan, H.; Liang, X.; Cao, D.; Shi, L.; Ding, P. Structural design of multilayer thermally conductive nanofibrillated cellulose hybrid film with electrical insulating and antistatic property. *J. Mater. Chem. C* **2018**, *6*, 7085–7091. [[CrossRef](#)]
8. Ma, H.; Hou, J.; Xiao, X.; Wan, R.; Ge, G.; Zheng, W.; Chen, C.; Cao, J.; Wang, J.; Liu, C.; et al. Self-healing electrical bioadhesive interface for electrophysiology recording. *J. Colloid Interface Sci.* **2024**, *654*, 639–648. [[CrossRef](#)]
9. Deng, J.; Yuk, H.; Wu, J.; Varela, C.; Chen, X.; Roche, E.; Guo, C.; Zhao, X. Electrical bioadhesive interface for bioelectronics. *Nat. Mater.* **2021**, *20*, 229–236. [[CrossRef](#)]
10. Zhou, T.; Yuk, H.; Hu, F.; Wu, J.; Tian, F.; Roh, H.; Shen, Z.; Gu, G.; Xu, J.; Lu, B.; et al. 3D printable high-performance conducting polymer hydrogel for all-hydrogel bioelectronic interfaces. *Nat. Mater.* **2023**, *22*, 895–902. [[CrossRef](#)]
11. Li, G.; Huang, K.; Deng, J.; Guo, M.; Cai, M.; Zhang, Y.; Guo, C. Highly conducting and stretchable double-network hydrogel for soft bioelectronics. *Adv. Mater.* **2022**, *34*, 2200261. [[CrossRef](#)]

12. Xue, Y.; Chen, X.; Wang, F.; Lin, J.; Liu, J. Mechanically-compliant bioelectronic interfaces through fatigue-resistant conducting polymer hydrogel coating. *Adv. Mater.* **2023**, *35*, 2304095. [[CrossRef](#)]
13. Tian, F.; Yu, J.; Wang, W.; Zhao, D.; Cao, J.; Zhao, Q.; Wang, F.; Yang, H.; Wu, Z.; Xu, J.; et al. Design of adhesive conducting PEDOT-MeOH:PSS/PDA neural interface via electropolymerization for ultrasmall implantable neural microelectrodes. *J. Colloid Interface Sci.* **2023**, *638*, 339–348. [[CrossRef](#)]
14. Yousefi, E.; Dolati, A.; Najafkhan, H. Preparation of robust antistatic waterborne polyurethane coating. *Prog. Org. Coat.* **2020**, *139*, 105450. [[CrossRef](#)]
15. Wang, H.; Liu, Y.; Fei, G.; Lan, J. Preparation, morphology, and conductivity of waterborne, nanostructured, cationic polyurethane/polypyrrole conductive coatings. *J. Appl. Polym. Sci.* **2014**, *132*, 41445. [[CrossRef](#)]
16. Shi, Y.; Tong, L.; Chu, J.; Li, X.; Zhang, B.; Wang, K. Hierarchical architecture of MXene/polypyrrole hybrid epoxy coating with superior anticorrosion and antistatic performance for Mg alloy. *Colloids Surface A* **2024**, *686*, 133359. [[CrossRef](#)]
17. Khezri, T.; Sharif, M.; Pourabas, B. Polythiophene-graphene oxide doped epoxy resin nanocomposites with enhanced electrical, mechanical and thermal properties. *RSC Adv.* **2016**, *6*, 93680. [[CrossRef](#)]
18. Lu, B.; Yuk, H.; Lin, S.; Jian, N.; Qu, K.; Xu, J.; Zhao, X. Pure PEDOT:PSS hydrogels. *Nat. Commun.* **2019**, *10*, 1043. [[CrossRef](#)]
19. Li, J.; Cao, J.; Lu, B.; Gu, G. 3D-printed PEDOT:PSS for soft robotics. *Nat. Rev. Mater.* **2023**, *8*, 604–622. [[CrossRef](#)]
20. Pranti, A.; Schander, A.; Bödecker, A.; Lang, W. PEDOT: PSS coating on gold microelectrodes with excellent stability and high charge injection capacity for chronic neural interfaces. *Sens. Actuators B-Chem.* **2018**, *275*, 382–393. [[CrossRef](#)]
21. Yuk, H.; Lu, B.; Lin, S.; Qu, K.; Xu, J.; Luo, J.; Zhao, X. 3D printing of conducting polymers. *Nat. Commun.* **2020**, *11*, 1604. [[CrossRef](#)]
22. Vedovatte, R.; Saccardo, M.; Costa, E.; Cava, C. PEDOT:PSS post-treated by DMSO using spin coating, roll-to-roll and immersion: A comparative study. *J. Mater. Sci. Mater. Electron.* **2020**, *31*, 317–323. [[CrossRef](#)]
23. Wang, F.; Xue, Y.; Chen, X.; Zhang, P.; Shan, L.; Duan, Q.; Xing, J.; Lan, Y.; Lu, B.; Liu, J. 3D printed implantable hydrogel bioelectronics for electrophysiological monitoring and electrical modulation. *Adv. Funct. Mater.* **2023**, *34*, 2314471. [[CrossRef](#)]
24. Yu, J.; Tian, F.; Wang, W.; Wan, R.; Cao, J.; Chen, C.; Zhao, D.; Liu, J.; Zhong, J.; Wang, F.; et al. Design of highly conductive, intrinsically stretchable, and 3D printable PEDOT:PSS hydrogels via PSS-chain engineering for bioelectronics. *Chem. Mater.* **2023**, *35*, 5936–5944. [[CrossRef](#)]
25. Cheng, T.; Wang, F.; Zhang, Y.; Li, L.; Gao, S.; Yang, X.; Wang, S.; Chen, S.; Lai, W. 3D printable conductive polymer hydrogels with ultra-high conductivity and superior stretchability for free-standing elastic all-gel supercapacitors. *Chem. Eng. J.* **2022**, *450*, 138311. [[CrossRef](#)]
26. Gao, W.; Dang, Z.; Liu, F.; Wang, S.; Zhang, D.; Yan, M. Preparation of antistatic epoxy resin coatings based on double comb-like quaternary ammonium salt polymers. *RSC Adv.* **2020**, *10*, 43523. [[CrossRef](#)]
27. Wang, J.; Zhang, C.; Du, Z.; Li, H.; Zou, W. Functionalization of MWCNTs with silver nanoparticles decorated polypyrrole and their application in antistatic and thermal conductive epoxy matrix nanocomposite. *RSC Adv.* **2016**, *6*, 31782–31789. [[CrossRef](#)]
28. Zhang, Z.; Chen, G.; Xue, Y.; Duan, Q.; Liang, X.; Lin, T.; Wu, Z.; Tan, Y.; Zhao, Q.; Zheng, W.; et al. Fatigue-resistant conducting polymer hydrogels as strain sensor for underwater robotics. *Adv. Funct. Mater.* **2023**, *33*, 2305705. [[CrossRef](#)]
29. Shen, Z.; Zhang, Z.; Zhang, N.; Li, J.; Zhou, P.; Hu, F.; Rong, Y.; Lu, B.; Gu, G. High-stretchability, ultralow-hysteresis conducting polymer hydrogel strain sensors for soft machines. *Adv. Mater.* **2022**, *34*, 2203650. [[CrossRef](#)]
30. Hu, F.; Xue, Y.; Xu, J.; Lu, B. PEDOT-based conducting polymer actuators. *Front. Robot. AI* **2019**, *6*, 114. [[CrossRef](#)]
31. Shen, Z.; Zhu, X.; Majidi, C.; Gu, G. Cutaneous ionogel mechanoreceptors for soft machines, physiological sensing, and amputee prostheses. *Adv. Mater.* **2021**, *33*, 2102069. [[CrossRef](#)]
32. Wan, R.; Liu, S.; Li, Z.; Li, G.; Li, J.; Xu, J.; Liu, X. 3D printing of highly conductive and strongly adhesive PEDOT:PSS hydrogel-based bioelectronic interface for accurate electromyography monitoring. *J. Colloid Interface Sci.* **2025**, *677*, 198–207. [[CrossRef](#)]
33. Luo, X.; Wan, R.; Zhang, Z.; Song, M.; Yan, L.; Xu, J.; Yang, H.; Lu, B. 3D-printed hydrogel-based flexible electrochromic device for wearable displays. *Adv. Sci.* **2024**, *2404679*. [[CrossRef](#)]
34. Yu, R.; Zhang, H.; Guo, B. Conductive biomaterials as bioactive wound dressing for wound healing and skin tissue engineering. *Nano-Micro Lett.* **2022**, *14*, 1. [[CrossRef](#)]
35. Zheng, W.; Wang, L.; Jiao, T.; Wu, Z.; Lin, T.; Ma, H.; Zhang, Z.; Xu, X.; Cao, J.; Zhong, J.; et al. A cost-effective, fast cooling, and efficient anti-inflammatory multilayered topological hydrogel patch for burn wound first aid. *Chem. Eng. J.* **2023**, *455*, 140553. [[CrossRef](#)]
36. Xue, Y.; Zhang, J.; Chen, X.; Zhang, J.; Chen, C.; Zhang, K.; Lin, J.; Guo, C.; Liu, J. Trigger-Detachable Hydrogel Adhesives for Bioelectronic Interfaces. *Adv. Funct. Mater.* **2021**, *31*, 2106446. [[CrossRef](#)]
37. Keene, S.; Lubrano, C.; Kazemzadeh, S.; Melianas, A.; Tuchman, Y.; Polino, G.; Scognamiglio, P.; Cina, L.; Salleo, A.; Salleo, A.; et al. A biohybrid synapse with neurotransmitter-mediated plasticity. *Nat. Mater.* **2020**, *19*, 969–973. [[CrossRef](#)]
38. Yu, J.; Wan, R.; Tian, F.; Cao, J.; Wang, W.; Liu, Q.; Yang, H.; Liu, J.; Liu, X.; Lin, T.; et al. 3D printing of robust high-performance conducting polymer hydrogel-based electrical bioadhesive interface for soft bioelectronics. *Small* **2024**, *20*, 2308778. [[CrossRef](#)]
39. Wang, J.; Li, Q.; Sun, X.; Wang, Y.; Zhuang, T.; Yan, J.; Wang, H. Ultra-high electrical conductivity in filler-free polymeric hydrogels toward thermoelectrics and electromagnetic interference shielding. *Adv. Mater.* **2022**, *34*, 2109904. [[CrossRef](#)]

40. Wu, Y.; Wang, Z.; Liu, X.; Zheng, Q.; Xue, Q.; Kim, J. Ultralight graphene foam/conductive polymer composites for exceptional electromagnetic interference shielding. *ACS Appl. Mater. Interfaces* **2017**, *9*, 9059–9069. [[CrossRef](#)]
41. Ghaderi, S.; Hosseini, H.; Haddadi, S.; Kamkar, M.; Arjmand, M. 3D printing of solvent-treated PEDOT:PSS inks for electromagnetic interference shielding. *J. Mater. Chem. A* **2023**, *11*, 16027. [[CrossRef](#)]
42. Wan, R.; Yu, J.; Quan, Z.; Ma, H.; Li, J.; Tian, F.; Wang, W.; Sun, Y.; Liu, J.; Gao, D.; et al. A reusable, healable, and biocompatible PEDOT:PSS hydrogel-based electrical bioadhesive interface for high-resolution electromyography monitoring and time-frequency analysis. *Chem. Eng. J.* **2024**, *490*, 151454. [[CrossRef](#)]
43. Xu, X.; Zhao, Q.; Liu, Q.; Qiu, J.; Li, J.; Zheng, W.; Cao, J.; Wang, L.; Wang, W.; Yuan, S.; et al. Full-spectrum-responsive Ti₄O₇-PVA nanocomposite hydrogel with ultrahigh evaporation rate for efficient solar steam generation. *Desalination* **2024**, *577*, 117400. [[CrossRef](#)]
44. Tian, Y.; Zhang, X.; Geng, H.; Yang, H.; Li, C.; Da, S.; Lu, S.; Wang, J.; Jia, S. Carbon nanotube/polyurethane films with high transparency, low sheet resistance and strong adhesion for antistatic application. *RSC Adv.* **2017**, *7*, 53018. [[CrossRef](#)]
45. Yuk, H.; Lu, B.; Zhao, X. Hydrogel bioelectronics. *Chem. Soc. Rev.* **2019**, *48*, 1642–1667. [[CrossRef](#)]
46. Li, J.; Cheng, F.; Li, H.; Zhang, H.; Wang, G.; Pan, D. Two-step deposition of Ag nanowires/Zn₂SnO₄ transparent conductive films for antistatic coatings. *RSC Adv.* **2021**, *11*, 14730–14736. [[CrossRef](#)]

Disclaimer/Publisher's Note: The statements, opinions and data contained in all publications are solely those of the individual author(s) and contributor(s) and not of MDPI and/or the editor(s). MDPI and/or the editor(s) disclaim responsibility for any injury to people or property resulting from any ideas, methods, instructions or products referred to in the content.